This article has been accepted for publication in a future issue of this journal, but has not been fully edited. Content may change prior to final publication. Citation information: DOI 10.1109/TSG.2016.2592978, IEEE Transactions on Smart Grid

Multi-Phase State Estimation Featuring Industrial-Grade Distribution Network Models

Izudin Džafić, *Senior Member*, *IEEE*, Rabih A. Jabr, *Fellow*, *IEEE*,
Indira Huseinagić, *Student Member*, *IEEE*, and Bikash C. Pal, *Fellow*, *IEEE*

***Abstract*—This paper proposes a novel implementation of a multi-phase distribution network state estimator which employs industrial-grade modeling of power components and measurements. Unlike the classical voltage-based and current-based state estimators, this paper presents the implementation details of a constrained weighted least squares state calculation method that includes standard three-phase state estimation capabilities in addition to practical modeling requirements from the industry; these requirements comprise multi-phase line configurations, unsymmetrical and incomplete transformer connections, power measurements on $\triangle$-connected loads, cumulative-type power measurements, line-to-line voltage magnitude measurements, and reversible line drop compensators. The enhanced modeling equips the estimator with capabilities that make it superior to a recently presented state-of-the-art distribution network load estimator that is currently used in real-life distribution management systems; comparative performance results demonstrate the advantage of the proposed estimator under practical measurement schemes.**

***Index Terms*—Power distribution, power system modeling, power system simulation, state estimation.**

NOMENCLATURE

δ_i^ϕ	Angle of $\underline{V}_i^\phi$.
$\Lambda(i)$	Set of nodes connected to node i by a branch.
ω_X^z	Weight for the measurement in set X and the associated nodes/phases in z.
θ_{ij}^{xy}	Angle of $\underline{Y}_{ij}^{xy}$.
B	Set of all branches; $B(ij)$ is the set of phases (out of a, b, c) in branch ij.
$COMP$	Set (with structure (ϕ, ij)) of phases in transformer branches having line drop compensators; $\phi \in \{a, b, c\}$ for a regulator on the Y-connected side and $\phi \in \{ab, bc, ca\}$ for a regulator on the Δ-connected side.
CT_P/CT_S	Primary/seconday current ratio of the current transformer in the compensator circuit.
I_{base-c}	Base current in the compensator circuit, corresponding to the base current in the line circuit I_{base}.
$\underline{I}_{Ci}^\phi$	Phasor current supplied by phase ϕ of the equivalent Y-connected capacitor bank at node i; $\phi \in \{a, b, c\}$.
$\underline{I}_{ij}^\phi$	Phasor current in phase ϕ of branch ij; $\phi \in \{a, b, c\}$.
$\underline{I}_{Li}^\phi$	Phasor current supplied to phase ϕ of the equivalent Y-connected load at node i; $\phi \in \{a, b, c\}$.
I_{X-im}^ϕ	Imaginary part of $\underline{I}_X^\phi$.
I_{X-re}^ϕ	Real part of $\underline{I}_X^\phi$.
I_X^ϕ	Magnitude of $\underline{I}_X^\phi$.
LPQ	Set (with structure (ϕ, i)) of phases at all the nodes with real/reactive load power; $\phi \in \{a, b, c\}$ for Y-connected loads and $\phi \in \{ab, bc, ca\}$ for Δ-connected loads.
MBC	Set (with structure (ϕ, ij)) of phases in the branches with current magnitude measurements; $\phi \in \{a, b, c\}$.
MBP	Set (with structure (ϕ, ij)) of phases in the branches with real power flow measurements; $\phi \in \{a, b, c\}$.
MBQ	Set (with structure (ϕ, ij)) of phases in the branches with reactive power flow measurements; $\phi \in \{a, b, c\}$.
$MCUMP$	Set of branches with cumulative real power flow measurements.
$MCUMQ$	Set of branches with cumulative reactive power flow measurements.
$MLGV$	Set (with structure (ϕ, i)) of phases at the nodes with line-to-ground voltage magnitude measurements; $\phi \in \{a, b, c\}$.
$MLLV$	Set (with structure (ϕ, i)) of phases at the nodes with line-to-line voltage magnitude measurements; $\phi \in \{ab, bc, ca\}$.
$N_{PT}/1$	Primary/seconday turns ratio of the potential transformer in the compensator circuit.
N	Set of all nodes; $N(i)$ is the set of phases (out of a, b, c) at node i.
P_{ij}^ϕ	Real power flow in phase ϕ of branch ij; $\phi \in \{a, b, c\}$.
P_{ij}^{CUM}	Cumulative real power flow in branch ij.
P_{Li}^ϕ	Real load power consumed in phase ϕ at node i; $\phi \in \{a, b, c\}$ for Y-connected loads and $\phi \in \{ab, bc, ca\}$ for Δ-connected loads.
Q_{Ci}^ϕ	Rated reactive power supplied by phase ϕ of the capacitor at node i; $\phi \in \{a, b, c\}$ for a Y-connected capacitor bank and $\phi \in \{ab, bc, ca\}$ for a Δ-connected capacitor bank.

I. Džafić and I. Huseinagić are with the International University of Sarajevo, Hrasnička cesta 15, 71210 Sarajevo, Bosnia (emails: idzafic@ieee.org, irustempasic@ius.edu.ba). The work of I. Džafić and I. Huseinagić is supported in part by Siemens Energy Automation, Nuremberg, Germany.

R. A. Jabr is with the Department of Electrical & Computer Engineering, American University of Beirut, P.O. Box 11-0236, Riad El- Solh / Beirut 1107 2020, Lebanon (email: rabih.jabr@aub.edu.lb).

B. C. Pal is with the Electrical and Electronic Engineering Department, Imperial College, London SW7 2AZ, U.K. (e-mail: b.pal@imperial.ac.uk).

This article has been accepted for publication in a future issue of this journal, but has not been fully edited. Content may change prior to final publication. Citation information: DOI 10.1109/TSG.2016.2592978, IEEE Transactions on Smart Grid

Q_{ij}^{ϕ}	Reactive power flow in phase ϕ of branch ij; $\phi \in \{a, b, c\}$.
Q_{ij}^{CUM}	Cumulative reactive power flow in branch ij.
Q_{Li}^{ϕ}	Reactive load power consumed in phase ϕ at node i; $\phi \in \{a, b, c\}$ for Y-connected loads and $\phi \in \{ab, bc, ca\}$ for Δ-connected loads.
R_{ij-c}^{ϕ}	Resistance (in per-unit) of the line drop compensator in phase ϕ at node i; the subscript V denotes the resistance calibrated in volts, and the subscript Ω denotes the resistance value in ohms.
$\underline{V}_i^{\phi}$	Phasor voltage across phase ϕ of node i; $\phi \in \{a, b, c\}$ for line-to-ground voltages and $\phi \in \{ab, bc, ca\}$ for line-to-line voltages.
V_{base-c}	Base voltage in the compensator circuit, corresponding to the base voltage in the line circuit V_{base}.
V_i^{ϕ}	Magnitude of $\underline{V}_i^{\phi}$.
VR_i^{ϕ}	Magnitude of the voltage across phase ϕ of the voltage relay at node i; $\phi \in \{a, b, c\}$ for a regulator on the Y-connected side and $\phi \in \{ab, bc, ca\}$ for a regulator on the Δ-connected side.
X_{ij-c}^{ϕ}	Reactance (in per-unit) of the line drop compensator in phase ϕ at node i; the subscript V denotes the reactance calibrated in volts, and the subscript Ω denotes the reactance value in ohms.
Y_{ij}^{xy}	Magnitude of $\underline{Y}_{ij}^{xy}$.
$\underline{Y}_{ij}^{xy}$	Element of the nodal admittance matrix corresponding to branch ij, and phases x and y.
Z_{base-c}	Base impedance in the compensator circuit.
Z_{y-M}^{x}	Measured value of the quantity Z_y^x.

I. Introduction

Distribution system state estimation (DSSE) is a key enabler in realizing modern smart grids; DSSE is a central function in distribution management systems as it provides input to various practical distribution automation functionalities amongst which are volt-var control and optimal feeder reconfiguration [1]. In comparison with transmission system state estimation, DSSE operates with relatively few real-time measurements and a multitude of load pseudo-measurements [2]–[5]. In fact, the load estimate is a main output of DSSE, and state estimation in distribution networks is commonly referred to as load estimation [6]. The state-of-the-art in three-phase radial and unsymmetrical distribution network load estimation has been recently presented in [7]. This paper reports further enhancements in the modeling of components and measurements as required by the power distribution industry; the resulting load estimator features industrial-grade models with capabilities that positively distinguish it from [7] in real-life operational scenarios.

One of the earliest DSSE techniques that accounts for the fundamental characteristics of distribution systems is the current balancing method [8], which is the precursor of the approach later developed in [7]. Another classical approach is based on implementing the transmission systems weighted least squares state estimator in distribution systems [9]; the implementation includes unbalanced conditions represented by

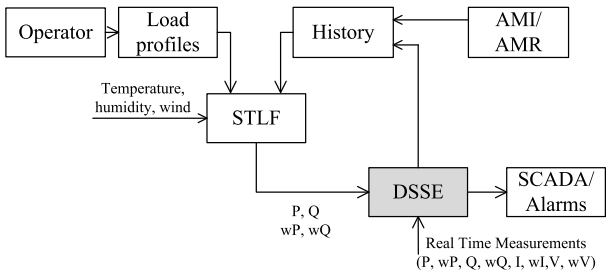

Fig. 1. Short-term load-forecasting for pseudo-measurement generation.

a three-phase feeder model and solidly-grounded Y-connected loads, line-to-ground voltage and branch current magnitude measurements, and load data as pseudo-measurements. A further extension of the method in [9] appeared in [10], which proposed a branch-current based state estimator. The branch-current based state estimator allows the decoupling of the Jacobian matrix on a per-phase basis when it is operated with Y-connected loads; this leads to computational performance improvements as compared to the voltage-based state estimator in [9]. However, in comparison with the voltage-based estimator, the current-based estimator neglects voltage magnitude measurements (except at the substation slack bus) and its computational advantage, which is attributed to decoupling, is limited to radial networks. Recent DSSE approaches are based on meta-heuristics [11] and Hamiltonian cycle theory [12].

Practical distribution system state estimation algorithms combine real-time measurements with historical (statistical) load data as pseudo-measurements [13]. In smart grids, data from the advanced metering infrastructure (AMI) and automated meter readings (AMRs) contribute to the computation of load pseudo-measurements and their weights [7]. AMR constitutes a collection of customer load information which is transmitted to the central computing unit at specified times of the day. As depicted in Fig. 1, AMI/AMR data together with previous DSSE results are combined with load profiles and meteorological conditions (temperature/humidity/wind speed) via a short-term load-forecasting (STLF) module that computes the pseudo-measurement data for processing by DSSE. The load profiles include hourly load values for different seasons, different day types (working day/holiday), and various load types (residential/industrial/commercial). Previously reported implementations of STLF employ probabilistic modeling [2], neural networks [4], machine learning [14], and a predictive database based on adaptive nonlinear auto-regressive exogenous load estimation [5]. The pseudo-measurements produced by STLF are further processed by the DSSE to produce a better estimate of the load that is consistent with the real-time SCADA measurements and the network model.

This paper presents the technical details of a DSSE solver which implements an equality-constrained formulation of the weighted least squares (WLS) method. The WLS objective includes different weights to differentiate between the quality of real-time and pseudo-measurements; real-time measurements are given a larger weight, whereas pseudo-measurements representing load forecasts are given a lower weight to allow a

This article has been accepted for publication in a future issue of this journal, but has not been fully edited. Content may change prior to final publication. Citation information: DOI 10.1109/TSG.2016.2592978, IEEE Transactions on Smart Grid

larger deviation between the estimated quantity and its corresponding pseudo-measurement value. The paper contributes industrial-grade models that feature:

- Multiphase line configurations in any topology (radial or meshed).
- Unsymmetrical Y- and △-connected loads.
- Unsymmetrical transformer connections with various clock numbers [15] that are in accordance with the British Standard (BS) and the International Electrotechnical Commission (IEC) Standard on power transformers [16].
- Y- and △-connected capacitor banks.
- Reversible voltage regulators with a line drop compensator circuit model; the corresponding transformer tap ratios can be set either in ganged or in non-ganged mode.

The measurement set employed by the DSSE solver includes:

- Voltage magnitude measurements: line-to-ground and line-to-line.
- Power measurements for Y- and △-connected loads, which normally represent forecast values.
- Branch measurements: current magnitude measurements, real/reactive power flow measurements on a phase, and real/reactive cumulative power measurements for all the branch phases.

The proposed DSSE method is distinguished from previous distribution state calculation algorithms [8]–[13] by allowing any combination of the features noted above. In comparison with a state-of-the-art real-time DSSE method that is currently used in distribution management systems [7], the proposed method has modeling advantages as detailed in Table I. Additionally, the proposed DSSE method removes a modeling limitation in [7], which necessitates line-to-ground voltage magnitude measurements to be available with current magnitude or real/reactive power measurements at the same location. The enhancements reported herein are in response to practical requests by the power distribution industry, and their technical implementation details in DSSE stand out as the original contribution of this paper.

The remainder of this paper is organized as follows. The modeling of the distribution network components and the constrained WLS solution are described in Sections II and III, respectively. Numerical results are given in Section IV, and include a comparison of the proposed DSSE method with the load estimator recently reported in [7]. Section V concludes the paper.

Table I
COMPARISON BETWEEN THE MODELING CAPABILITIES OF THE STATE ESTIMATION METHODS

Type of Measurement	Ref. [7]	Proposed DSSE
Cumulative active power	No	Yes
Cumulative reactive power	No	Yes
Current magnitude	Yes	Yes
Active power	Yes	Yes
Reactive power	Yes	Yes
Line-to-ground voltage magnitude	No	Yes
Line-to-line voltage magnitude	No	Yes
Tap changer $t_{\triangle}$	No	Yes
Tap changer t_Y	No	Yes
Multi-slack	No	Yes
Measurement in loops	No	Yes

II. DISTRIBUTION NETWORK COMPONENT MODELING

A. Branches: Lines and Transformers (Fig. 2)

The modeling of three-phase, two-phase, or single-phase overhead and underground lines is carried out using the standard π-equivalent approach, leading to the following nodal matrix equation (1) for branch currents [17]. Each sub-matrix in (1), for instance $\underline{Y}_{ii}$ as displayed in (3), is nominally a 3×3 matrix with complex values; when a line segment has missing phases, the corresponding rows and columns in the admittance matrix in (1) will be zero.

$$\begin{bmatrix} \underline{I}_{ij} \\ \underline{I}_{ji} \end{bmatrix} = \begin{bmatrix} \underline{Y}_{ii} & \underline{Y}_{ij} \\ \underline{Y}_{ji} & \underline{Y}_{jj} \end{bmatrix} \begin{bmatrix} \underline{V}_{i} \\ \underline{V}_{j} \end{bmatrix} \tag{1}$$

$$\underline{I}_{ij} = \begin{bmatrix} \underline{I}_{ij}^{a} \\ \underline{I}_{ij}^{b} \\ \underline{I}_{ij}^{c} \end{bmatrix}, \ \underline{V}_{i} = \begin{bmatrix} \underline{V}_{i}^{a} \\ \underline{V}_{i}^{b} \\ \underline{V}_{i}^{c} \end{bmatrix} \tag{2}$$

$$\underline{Y}_{ii} = \begin{bmatrix} \underline{Y}_{ii}^{aa} & \underline{Y}_{ii}^{ab} & \underline{Y}_{ii}^{ac} \\ \underline{Y}_{ii}^{ba} & \underline{Y}_{ii}^{bb} & \underline{Y}_{ii}^{bc} \\ \underline{Y}_{ii}^{ca} & \underline{Y}_{ii}^{cb} & \underline{Y}_{ii}^{cc} \end{bmatrix} \tag{3}$$

Using (1), the complex current in any phase $\phi = x = \{a, b, c\}$ between nodes i and j can be expressed by (4), with the corresponding expressions for the real and imaginary branch current components given by (5) and (6), respectively:

$$\begin{aligned} \underline{I}_{ij}^{\phi} = \underline{I}_{ij}^{x} = & \sum_{y\in\{a,b,c\}} Y_{ii}^{xy} V_i^y \exp(j(\theta_{ii}^{xy} + \delta_i^y)) \\ & + \sum_{y\in\{a,b,c\}} Y_{ij}^{xy} V_j^y \exp(j(\theta_{ij}^{xy} + \delta_j^y)) \end{aligned} \tag{4}$$

$$\begin{aligned} I_{ij-re}^{\phi} = & \sum_{y\in\{a,b,c\}} Y_{ii}^{\phi y} V_i^y \cos(\theta_{ii}^{\phi y} + \delta_i^y) \\ & + \sum_{y\in\{a,b,c\}} Y_{ij}^{\phi y} V_j^y \cos(\theta_{ij}^{\phi y} + \delta_j^y), \quad \phi \in B(ij) \end{aligned} \tag{5}$$

$$\begin{aligned} I_{ij-im}^{\phi} = & \sum_{y\in\{a,b,c\}} Y_{ii}^{\phi y} V_i^y \sin(\theta_{ii}^{\phi y} + \delta_i^y) \\ & + \sum_{y\in\{a,b,c\}} Y_{ij}^{\phi y} V_j^y \sin(\theta_{ij}^{\phi y} + \delta_j^y), \quad \phi \in B(ij) \end{aligned} \tag{6}$$

Transformer connections, which can be comprised either of three single-phase units or one three-phase unit, are modeled with nodal admittance matrices (1) using the approach in [15]. This approach allows modeling 1) different leakage impedances in the transformer bank, 2) incomplete three-phase transformer banks (e.g., open delta-open delta and open wye-open delta), 3) different clock numbers as defined in the BS and IEC Standard on power transformers [16], 4) grounding impedances for neutral points, and 5) different transformer tap

This article has been accepted for publication in a future issue of this journal, but has not been fully edited. Content may change prior to final publication. Citation information: DOI 10.1109/TSG.2016.2592978, IEEE Transactions on Smart Grid

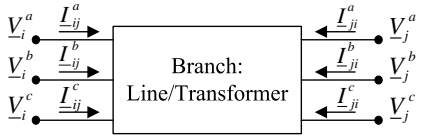

Fig. 2. Branch representation in DSSE.

ratios that implement per-phase voltage control. The transformer tap ratios can be controlled either by a non-ganged voltage regulator where the tap ratios on the different phases can take different values, or by a ganged regulator where all the tap ratios take the same value.

For each voltage regulator phase, a line drop compensator as shown in Fig. 3 is modeled. The compensator is an analog circuit, which serves as a scale model of the line circuit [18]; the per-unit compensator impedance is normally set equal to the per-unit line impedance from the regulator to the load bus where the voltage is to be controlled. In practice, the most critical setting of the compensator is its series impedance $(R^{\phi}_{ij-cV} + jX^{\phi}_{ij-cV})$ calibrated in volts. With the base quantities defined for the compensator circuit as in (7)-(9), the compensator impedance values in ohms and in per-unit are given by (10) and (11), respectively. The phasor voltage on the voltage relay (in per-unit) can be then expressed in terms of the line circuit voltage and current (12); with the compensator impedance properly calibrated, the per-unit relay voltage would match the per-unit voltage at the load bus. The magnitude of the relay voltage VR^{ϕ}_{j} is therefore set to the desired voltage magnitude at the load bus. In the DDSE implementation, the voltage controlled side is automatically chosen as the one in the direction of active power flow.

$$V_{base-c} = \frac{V_{base}}{N_{PT}} \tag{7}$$

$$I_{base-c} = \frac{CT_S}{CT_P} I_{base} \tag{8}$$

$$Z_{base-c} = \frac{V_{base-c}}{I_{base-c}} = \frac{CT_P}{CT_S N_{PT}} \frac{V_{base}}{I_{base}} \tag{9}$$

$$R^{\phi}_{ij-c\Omega} + jX^{\phi}_{ij-c\Omega} = \frac{R^{\phi}_{ij-cV} + jX^{\phi}_{ij-cV}}{I_{base}} \frac{CT_P}{CT_S} \tag{10}$$

$$R^{\phi}_{ij-c} + jX^{\phi}_{ij-c} = \frac{R^{\phi}_{ij-c\Omega} + jX^{\phi}_{ij-c\Omega}}{Z_{base-c}} \tag{11}$$

$$\underline{VR}^{\phi}_{j} = \underline{V}^{\phi}_{j} + (R^{\phi}_{ij-c} + jX^{\phi}_{ij-c})\underline{I}^{\phi}_{ji} \tag{12}$$

B. Capacitor Banks (Fig. 4)

1) Y-Connected Capacitor Bank: With $Q^{\phi}_{C} \geq 0$ denoting the rated reactive power at nominal voltage, the phasor current injected into phase $\phi \in \{a, b, c\}$ at node *i* is given by (13), with the real and imaginary components given by (14) and (15), respectively. Following industry practice, the Y-connected capacitor bank is assumed to be solidly grounded and the voltages in (13)-(15) are line-to-ground.

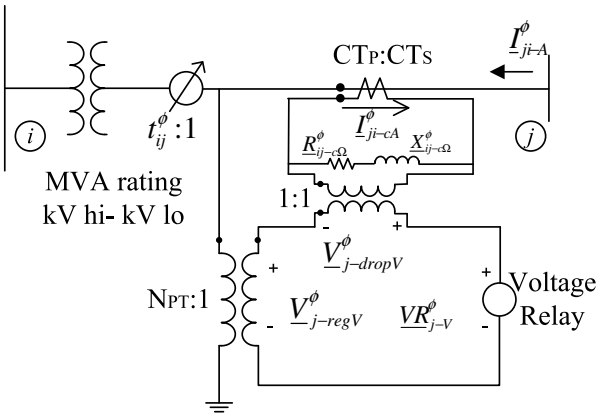

Fig. 3. Line drop compensator circuit.

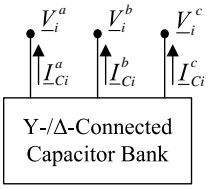

Fig. 4. Capacitor bank representation in DSSE.

$$\underline{I}^{\phi}_{Ci} = -jQ^{\phi}_{Ci}\underline{V}^{\phi}_{i} = -jQ^{\phi}_{Ci}V^{\phi}_{i}\exp(j\delta^{\phi}_{i}) \tag{13}$$

$$I^{\phi}_{Ci-re} = Q^{\phi}_{Ci}V^{\phi}_{i}\sin(\delta^{\phi}_{i}) \tag{14}$$

$$I^{\phi}_{Ci-im} = -Q^{\phi}_{Ci}V^{\phi}_{i}\cos(\delta^{\phi}_{i}) \tag{15}$$

2) △-Connected Capacitor Bank: Let $\phi = x \in \{a, b, c\}$, $xy \in \{ab, bc, ca\}$, and $zx \in \{ca, ab, bc\}$. The phasor current in phase *xy* of the △-connected capacitor bank at node *i* is given by (16); the real and imaginary components are given by (17) and (18), respectively. The corresponding current injected into phase ϕ of node *i* and its real/imaginary components are computed using KCL as in (19)-(21).

$$\begin{aligned} \underline{I}^{xy}_{Ci} &= -jQ^{xy}_{Ci}(\underline{V}^{x}_{i} - \underline{V}^{y}_{i}) \\ &= -jQ^{xy}_{Ci}(V^{x}_{i}\exp(j\delta^{x}_{i}) - V^{y}_{i}\exp(j\delta^{y}_{i})) \end{aligned} \tag{16}$$

$$I^{xy}_{Ci-re} = Q^{xy}_{Ci}\left(V^{x}_{i}\sin(\delta^{x}_{i}) - V^{y}_{i}\sin(\delta^{y}_{i})\right) \tag{17}$$

$$I^{xy}_{Ci-im} = -Q^{xy}_{Ci}\left(V^{x}_{i}\cos(\delta^{x}_{i}) - V^{y}_{i}\cos(\delta^{y}_{i})\right) \tag{18}$$

$$\underline{I}^{\phi}_{Ci} = \underline{I}^{x}_{Ci} = \underline{I}^{zx}_{Ci} - \underline{I}^{xy}_{Ci} \tag{19}$$

$$I^{\phi}_{Ci-re} = I^{zx}_{Ci-re} - I^{xy}_{Ci-re} \tag{20}$$

$$I^{\phi}_{Ci-im} = I^{zx}_{Ci-im} - I^{xy}_{Ci-im} \tag{21}$$

This article has been accepted for publication in a future issue of this journal, but has not been fully edited. Content may change prior to final publication. Citation information: DOI 10.1109/TSG.2016.2592978, IEEE Transactions on Smart Grid

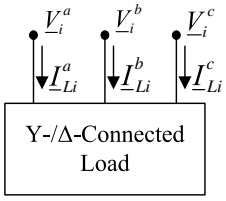

Fig. 5. Load representation in DSSE.

C. Loads (Fig. 5)

1) Y-Connected Load: Consider a solidly grounded Y-connected load at node *i*, which is specified by a per-phase complex power of $P_{Li}^{\phi} + jQ_{Li}^{\phi}$. The phasor current drawn by phase $\phi \in \{a, b, c\}$ is given by (22). The corresponding real and imaginary components of the load currents are given by (23) and (24), respectively.

$$\underline{I}_{Li}^{\phi} = \frac{P_{Li}^{\phi} - jQ_{Li}^{\phi}}{(\underline{V}_i^{\phi})^*} = \frac{P_{Li}^{\phi} - jQ_{Li}^{\phi}}{V_i^{\phi}\exp(-j\delta_i^{\phi})} \tag{22}$$

$$I_{Li-re}^{\phi} = \frac{P_{Li}^{\phi}}{V_i^{\phi}}\cos(\delta_i^{\phi}) + \frac{Q_{Li}^{\phi}}{V_i^{\phi}}\sin(\delta_i^{\phi}) \tag{23}$$

$$I_{Li-im}^{\phi} = \frac{P_{Li}^{\phi}}{V_i^{\phi}}\sin(\delta_i^{\phi}) - \frac{Q_{Li}^{\phi}}{V_i^{\phi}}\cos(\delta_i^{\phi}) \tag{24}$$

2) △-Connected Load: Let $\phi = x \in \{a, b, c\}$, $xy \in \{ab, bc, ca\}$, and $zx \in \{ca, ab, bc\}$. The phasor current drawn by phase *xy* of the △-connected load at node *i* is given by (25); the real and imaginary components are given by (26) and (27), respectively. The corresponding current drawn by phase ϕ of node *i* and its real/imaginary components are calculated using KCL as in (28)-(30).

$$\underline{I}_{Li}^{xy} = \frac{P_{Li}^{xy} - jQ_{Li}^{xy}}{(\underline{V}_i^{x} - \underline{V}_i^{y})^*} = \frac{P_{Li}^{xy} - jQ_{Li}^{xy}}{V_i^{x}\exp(-j\delta_i^{x}) - V_i^{y}\exp(-j\delta_i^{y})} \tag{25}$$

$$\begin{aligned} I_{Li-re}^{xy} = &\frac{P_{Li}^{xy}\left(V_i^x\cos(\delta_i^x) - V_i^y\cos(\delta_i^y)\right)}{(V_i^x)^2 + (V_i^y)^2 - 2V_i^xV_i^y\cos(\delta_i^x - \delta_i^y)} \\ &+\frac{Q_{Li}^{xy}\left(V_i^x\sin(\delta_i^x) - V_i^y\sin(\delta_i^y)\right)}{(V_i^x)^2 + (V_i^y)^2 - 2V_i^xV_i^y\cos(\delta_i^x - \delta_i^y)} \end{aligned} \tag{26}$$

$$\begin{aligned} I_{Li-im}^{xy} = &\frac{P_{Li}^{xy}\left(V_i^x\sin(\delta_i^x) - V_i^y\sin(\delta_i^y)\right)}{(V_i^x)^2 + (V_i^y)^2 - 2V_i^xV_i^y\cos(\delta_i^x - \delta_i^y)} \\ &-\frac{Q_{Li}^{xy}\left(V_i^x\cos(\delta_i^x) - V_i^y\cos(\delta_i^y)\right)}{(V_i^x)^2 + (V_i^y)^2 - 2V_i^xV_i^y\cos(\delta_i^x - \delta_i^y)} \end{aligned} \tag{27}$$

$$\underline{I}_{Li}^{\phi} = \underline{I}_{Li}^{x} = \underline{I}_{Li}^{xy} - \underline{I}_{Li}^{zx} \tag{28}$$

$$I_{Li-re}^{\phi} = I_{Li-re}^{xy} - I_{Li-re}^{zx} \tag{29}$$

$$I_{Li-im}^{\phi} = I_{Li-im}^{xy} - I_{Li-im}^{zx} \tag{30}$$

III. Weighted Least Squares Estimation

A. Equality-Constrained Optimization

Distribution system state estimation aims to compute the state vector of the network given by the line-to-ground voltage phasors and transformer tap ratios. The most likely state of the system is based on quantities that are measured and is commonly computed by maximum likelihood estimation [19]; this translates into minimizing a weighted sum of squares of measurement residuals, where the residual at the solution point is the difference between the actual measurement and its estimated value. DSSE can be cast as an equality-constrained optimization problem: minimize (31) subject to (32)-(40). The measured quantities that appear in (31) are: real/reactive load power measurements at all load carrying nodes, real/reactive branch power flow measurements, real/reactive cumulative branch power flow measurements, line-to-ground/line-to-line voltage magnitude measurements, and branch current magnitude measurements. The load real/reactive power measurements are practically pseudo-measurements obtained from load forecasts, and they have a lower weight associated with them. Additionally, slack voltages at the power injection node are always measured.

Objective function:

$$\begin{aligned} f \;=\; \frac{1}{2}\Bigg[&\sum_{(\phi,i)\in LPQ} \omega_{LPQ}^{(\phi,i)}(P_{Li}^{\phi} - P_{Li-M}^{\phi})^2 \\ &+ \sum_{(\phi,i)\in LPQ} \omega_{LPQ}^{(\phi,i)}(Q_{Li}^{\phi} - Q_{Li-M}^{\phi})^2 \\ &+ \sum_{(\phi,ij)\in MBP} \omega_{BP}^{(\phi,ij)}(P_{ij}^{\phi} - P_{ij-M}^{\phi})^2 \\ &+ \sum_{(\phi,ij)\in MBQ} \omega_{BQ}^{(\phi,ij)}(Q_{ij}^{\phi} - Q_{ij-M}^{\phi})^2 \\ &+ \sum_{ij\in MCUMP} \omega_{CUMP}^{ij}(P_{ij}^{CUM} - P_{ij-M}^{CUM})^2 \\ &+ \sum_{ij\in MCUMQ} \omega_{CUMQ}^{ij}(Q_{ij}^{CUM} - Q_{ij-M}^{CUM})^2 \\ &+ \sum_{(\phi,i)\in MLGV} \omega_{LGV}^{(\phi,i)}(V_i^{\phi} - V_{i-M}^{\phi})^2 \\ &+ \sum_{(\phi,i)\in MLLV} \omega_{LLV}^{(\phi,i)}(V_i^{\phi} - V_{i-M}^{\phi})^2 \\ &+ \sum_{(\phi,ij)\in MBC} \omega_{BC}^{(\phi,ij)}(I_{ij}^{\phi} - I_{ij-M}^{\phi})^2 \Bigg] \end{aligned} \tag{31}$$

In practice, the weights in (31) that correspond to SCADA measurements are set by the operator based on experience, whereas the weights of the pseudo-measurements come from the short-term load forecasting tool that gives the pseudo-measurement load values (c.f. Fig. 1).

Constraints:

1. KCL at the phase of each node (32)-(33), with individual currents defined by the equations (5), (6), (14), (15), (20), (21), (23), (24), (29), and (30).

This article has been accepted for publication in a future issue of this journal, but has not been fully edited. Content may change prior to final publication. Citation information: DOI 10.1109/TSG.2016.2592978, IEEE Transactions on Smart Grid

$$\sum_{j\in\Lambda(i)} I^{\phi}_{ij-re} + I^{\phi}_{Li-re} - I^{\phi}_{Ci-re} = 0,\ \forall i \in N,\ \phi \in N(i) \quad (32)$$

$$\sum_{j\in\Lambda(i)} I^{\phi}_{ij-im} + I^{\phi}_{Li-im} - I^{\phi}_{Ci-im} = 0, \forall i \in N, \phi \in N(i) \quad (33)$$

2. Real and reactive branch power flows (34)-(35) corresponding to branch power flow measurements.

$$P^{\phi}_{ij} - V^{\phi}_i I^{\phi}_{ij-re}\cos(\delta^{\phi}_i) - V^{\phi}_i I^{\phi}_{ij-im}\sin(\delta^{\phi}_i) = 0, \quad \forall(\phi, ij) \in MBP \quad (34)$$

$$Q^{\phi}_{ij} - V^{\phi}_i I^{\phi}_{ij-re}\sin(\delta^{\phi}_i) + V^{\phi}_i I^{\phi}_{ij-im}\cos(\delta^{\phi}_i) = 0, \quad \forall(\phi, ij) \in MBQ \quad (35)$$

3. Real and reactive cumulative branch power flows (36)-(37) corresponding to the cumulative branch power flow measurements; a cumulative power measurement involves the real/reactive power on all phases of a particular branch.

$$P^{CUM}_{ij} - \sum_{\phi\in B(ij)} P^{\phi}_{ij} = 0,\ \forall ij \in MCUMP$$
$$P^{\phi}_{ij} = V^{\phi}_i I^{\phi}_{ij-re}\cos(\delta^{\phi}_i) + V^{\phi}_i I^{\phi}_{ij-im}\sin(\delta^{\phi}_i), \quad \forall\phi \in B(ij) \quad (36)$$

$$Q^{CUM}_{ij} - \sum_{\phi\in B(ij)} Q^{\phi}_{ij} = 0,\ \forall ij \in MCUMQ$$
$$Q^{\phi}_{ij} = V^{\phi}_i I^{\phi}_{ij-re}\sin(\delta^{\phi}_i) - V^{\phi}_i I^{\phi}_{ij-im}\cos(\delta^{\phi}_i), \quad \forall\phi \in B(ij) \quad (37)$$

4. Squared line voltage magnitude corresponding to the line-to-line voltage magnitude measurements (38), and expressed in terms of the line-to-ground voltage magnitudes and angles.

$$(V^{xy}_i)^2 - (V^{x}_i)^2 - (V^{y}_i)^2 + 2V^{x}_i V^{y}_i \cos(\delta^{x}_i - \delta^{y}_i) = 0, \quad \forall(\phi, i) \in MLLV,\ \phi = xy \in \{ab, bc, ca\} \quad (38)$$

5. Squared branch current magnitude corresponding to the branch current magnitude measurements (39), and expressed in terms of the real and imaginary components.

$$(I^{\phi}_{ij})^2 - (I^{\phi}_{ij-re})^2 - (I^{\phi}_{ij-im})^2 = 0,\ \forall(\phi, i) \in MBC \quad (39)$$

6. Squared voltage magnitude at the compensator voltage relay (40), where the VR^{ϕ}_j has a set value; (40) is derived from (12).

$$(VR^{\phi}_j)^2 = \left(V^{\phi}_j\cos(\delta^{\phi}_j) + R^{\phi}_{ij-c}I^{\phi}_{ji-re} - X^{\phi}_{ij-c}I^{\phi}_{ji-im}\right)^2 + \left(V^{\phi}_j\sin(\delta^{\phi}_j) + R^{\phi}_{ij-c}I^{\phi}_{ji-im} + X^{\phi}_{ij-c}I^{\phi}_{ji-re}\right)^2, \quad \forall(\phi, ij) \in COMP \quad (40)$$

B. Solution Approach

The above equality constrained optimization problem (minimize (31) subject to (32)-(40)) can be written in compact form [20]:

$$\min_{\zeta\in\mathbb{R}^n} \{f(\zeta) | g(\zeta) = 0\} \quad (41)$$

where $f : \mathbb{R}^n \to \mathbb{R}$, $g : \mathbb{R}^n \to \mathbb{R}^m$, and the vector of variables ζ includes all the variables that appear in the constrained WLS problem formulation. The WLS objective function can be alternatively expressed as (42), where W is a diagonal matrix of weights:

$$f(\zeta) = \frac{1}{2}(\zeta - \zeta_M)^T W (\zeta - \zeta_M) \quad (42)$$

The first-order necessary conditions for optimality are [20]:

$$\nabla f(\zeta^{\bigstar}) + J(\zeta^{\bigstar})^T \lambda^{\bigstar} = 0 \quad (43)$$
$$g(\zeta^{\bigstar}) = 0 \quad (44)$$

where $\zeta^{\bigstar}$ is a regular point of $g(\zeta) = 0$, $J(\zeta^{\bigstar})$ is the Jacobian of g evaluated at $\zeta^{\bigstar}$, and $\lambda^{\bigstar}$ is the vector of Lagrange multipliers for $g(\zeta) = 0$.

Applying the Gauss-Newton technique [19], the nonlinear set of equations (43)-(44) is solved iteratively by means of computing a solution to the linear system (45) and then updating ζ via (46):

$$\begin{bmatrix} W & J(\zeta^{(\nu)})^T \\ J(\zeta^{(\nu)}) & 0 \end{bmatrix} \begin{bmatrix} \Delta\zeta^{(\nu)} \\ \lambda^{(\nu+1)} \end{bmatrix} = - \begin{bmatrix} W(\zeta^{(\nu)} - \zeta_M) \\ g(x^{(\nu)}) \end{bmatrix} \quad (45)$$

$$\zeta^{(\nu+1)} = \zeta^{(\nu)} + \Delta\zeta^{(\nu)} \quad (46)$$

The iterations start with an initial vector for $\zeta^{(0)}$ and continue until $\left|\Delta\zeta^{(\nu)}\right|_{\infty}$ is less than a pre-specified tolerance. The DSSE was developed as an equality-constrained WLS problem; this is motivated by: (i) The presence of zero injections. Given the use of load pseudo-measurements in addition to the real-time SCADA measurements, a large difference in weight values is needed, with the weight ratio of pseudo-measurements to real-time measurements in the range 1/100 to 1/1000. This implies that the zero injection measurement would require even a higher weight when using the Gain matrix approach (classical Gauss-Newton WLS), possibly leading to ill-conditioning. In the equality-constrained estimator, the zero injections are exactly modeled using equality constraints (32)-(33), without assigning weights to them in the objective function. As noted in [19] (section 3.5), the equality-constrained WLS approach allows simple scaling of the weight matrix W so that the indefinite coefficient matrix in (45) will have a very low condition number; this is not the case with the conventional WLS approach, where scaling the objective function has no effect on the condition number of the classical gain matrix ($G = H^T W H$). To factor the symmetric indefinite matrix in (45) while preserving symmetry, a Bunch-Kaufman

This article has been accepted for publication in a future issue of this journal, but has not been fully edited. Content may change prior to final publication. Citation information: DOI 10.1109/TSG.2016.2592978, IEEE Transactions on Smart Grid

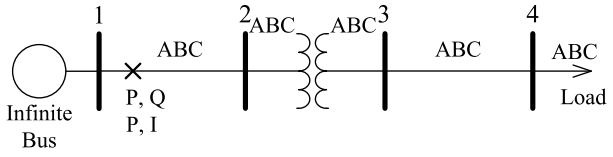

Fig. 6. IEEE 4-node test feeder with a closed transformer connection.

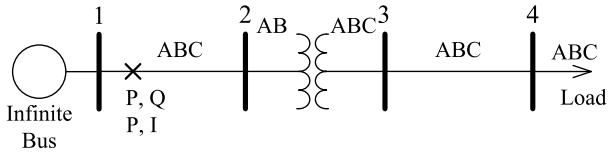

Fig. 7. IEEE 4-node test feeder with an open transformer connection.

block-pivot approach that resorts to 1×1 and 2×2 pivots is employed. Additionally, the number of non-zeros in the coefficient matrix of the equality-constrained estimator is significantly smaller than in the classical gain matrix. (ii) The fact that the equality-constrained WLS formulation simplifies the implementation and maintenance of the software, specifically with the detailed component models and measurement options that are adopted in DSSE.

IV. Numerical Results

The proposed DSSE method was programmed using C++ and compiled into Matlab executable files (MEX-files); the DSSE programs can be downloaded from [21] for the replication of test results. Comparison is carried out with the load estimator in [7], which is an industrial DSSE software package that is based on iterating between WLS-based load scaling and power flow solution. The results are reported on the IEEE 4-node test feeder designed to test the transformer connections and unbalanced loading, and the 123-node test feeder to show the DSSE functionalities relative to [7].

A. IEEE 4-node Test System

The IEEE 4-node test feeder is used here to demonstrate part of the DNToolbox features, and to validate the solution with the power flow benchmark results for unbalanced loading as reported in [22]. Three cases are considered: two with closed transformer step down connections (Yg-Yg and $\triangle$-Yg) as in Fig. 6, and one with a step-down open transformer connection (open Yg-open $\triangle$) as in Fig. 7. The measurement set consists of the three-phase line-to-ground voltage magnitudes at node 1 (7.2 kV magnitude for each phase), the real and reactive load power at node 4, and either the real and the reactive power (P,Q) or the real power and the current magnitude (P,I) in the three phases of the line connecting node 1 to node 2. For the purpose of validation, all these measurements have been directly obtained or computed using the power flow solution data in [22]. The load measurement is practically a pseudo-measurement representing a forecast value; this is reflected by assigning a relatively large weight of 1000 to the actual voltage measurements, a weight of 100 to actual branch measurements ((P,Q), (P,I)), and a relatively low weight of 1 to the pseudo-measurements. The fact that the pseudo-measurements have less weight allows the DSSE solution to produce a load estimate that differs from and improves on the pseudo-measurement value. Different levels of load forecast error values have been investigated ($\pm 5\%$, $\pm 10\%$, $\pm 15\%$, $\pm 20\%$), and the DSSE results are compared with the published power flow results. Due to space limitations, a subset of the results is shown herein and the complete result set is made available online [23].

1) Closed Transformer Connection: For the step-down Yg-Yg transformer connection, the three-phase voltage phasors at all nodes (Table II) and the three-phase currents in all branches are published in [22]; the true values of the real and reactive flows in the branch connecting node 1 to node 2 together with the current magnitudes are reported in Table III. The error in load forecast is assumed at $+20\%$ relative to the true load values in [22], giving the pseudo-measurements in Table IV. Two measurement scenarios are considered. In the first

Table II
Three-Phase Voltage Phasors for the Yg-Yg Transformer Connection [22]

Node-i	V_i^a[kV]	V_i^b[kV]	V_i^c [kV]	δ_i^a	δ_i^b	δ_i^c
Node-1	7.200	7.200	7.200	0.0°	–120.0°	120.0°
Node-2	7.164	7.110	7.082	–0.1°	–120.2°	119.3°
Node-3	2.305	2.255	2.203	–2.3°	–123.6°	114.8°
Node-4	2.175	1.930	1.833	–4.1°	–126.8°	102.8°

Table III
True Values of Branch Measurements for the Yg-Yg Transformer Connection

Phase-ϕ	P_{12}^{ϕ} [kW]	Q_{12}^{ϕ} [kVAr]	I_{12}^{ϕ} [A]
Phase-A	1341.6	971.6	230.1
Phase-B	2096.0	1342.5	345.7
Phase-C	2672.4	1895.8	455.1

Table IV
Unbalanced Load at Node 4 with 20% Error for the Closed Transformer Connections

Phase-ϕ	P_{L4}^{ϕ} [kW]	Q_{L4}^{ϕ} [kVAr]
Phase-A	1530.0	948.21
Phase-B	2160.0	1046.14
Phase-C	2850.0	936.75

Table V
DSSE Voltage Magnitude Results for the Yg-Yg Transformer Connection: (P,Q) Branch Measurements and +20% Error in the Load Forecast

Node-i	DSSE Results [kV]			Error [%]		
	V_i^a	V_i^b	V_i^c	ΔV_i^a	ΔV_i^b	ΔV_i^c
Node-1	7.200	7.202	7.201	0.00	0.03	0.01
Node-2	7.164	7.113	7.083	0.00	0.04	0.01
Node-3	2.306	2.255	2.203	0.04	0.00	0.00
Node-4	2.175	1.931	1.833	0.00	0.05	0.00

This article has been accepted for publication in a future issue of this journal, but has not been fully edited. Content may change prior to final publication. Citation information: DOI 10.1109/TSG.2016.2592978, IEEE Transactions on Smart Grid

Table VI
DSSE ESTIMATED MEASUREMENT RESULTS FOR THE YG-YG TRANSFORMER CONNECTION: (P,Q) BRANCH MEASUREMENTS AND +20% ERROR IN THE LOAD FORECAST

Phase-ϕ	DSSE Results		Error [%]	
	P_{12}^{ϕ} [kW]	Q_{12}^{ϕ} [kVAr]	ΔP_{12}^{ϕ}	ΔQ_{12}^{ϕ}
Phase-A	1341.6	971.6	0.00	0.00
Phase-B	2096.0	1342.5	0.00	0.00
Phase-C	2672.4	1895.8	0.00	0.00

Table VII
DSSE VOLTAGE MAGNITUDE RESULTS FOR THE YG-YG TRANSFORMER CONNECTION: (P,I) BRANCH MEASUREMENTS AND +20% ERROR IN THE LOAD FORECAST

Node-i	DSSE Results [kV]			Error [%]		
	V_i^a	V_i^b	V_i^c	ΔV_i^a	ΔV_i^b	ΔV_i^c
Node-1	7.201	7.202	7.202	0.01	0.03	0.03
Node-2	7.165	7.113	7.084	0.01	0.04	0.03
Node-3	2.306	2.255	2.303	0.04	0.00	0.00
Node-4	2.175	1.931	1.833	0.00	0.05	0.00

scenario, the measurements on the first branch consist of the real and reactive power flows (P,Q) in all phases. The DSSE voltage estimates are given in Table V together with the error in percent relative to the true value: $100\times$|estimated_value – true_valuel/true_value. Table VI shows the corresponding values of the estimated branch measurements and the relative errors. Tables VII and VIII show similar values for the second measurement scenario where the branch measurements consist of the real power flows and the current magnitudes (P,I) in the three phases. In both scenarios, the maximum relative error is not more than 0.05%.

2) Summary of Cases: The above testing procedure was repeated for three transformer connection types (Yg-Yg, △-Yg, and open Yg-open △), two branch measurement types, and four load error values; Table IX includes a summary of the maximum relative voltage error values.

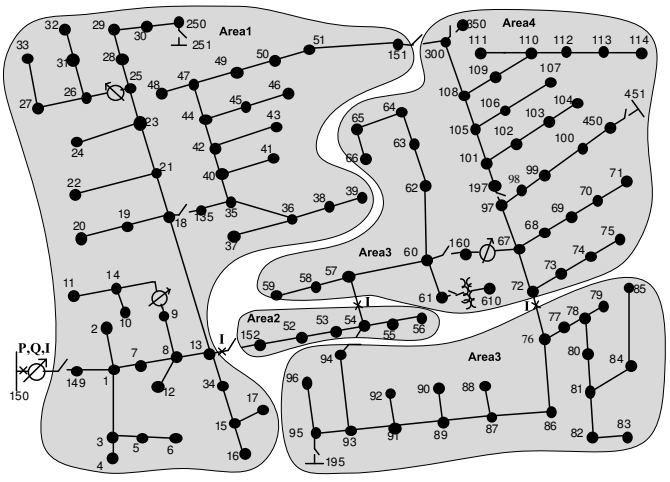

Fig. 8. IEEE 123-node test system.

Table VIII
DSSE ESTIMATED MEASUREMENT RESULTS FOR THE YG-YG TRANSFORMER CONNECTION: (P,I) BRANCH MEASUREMENTS AND +20% ERROR IN THE LOAD FORECAST

Phase-ϕ	DSSE Results		Error [%]	
	P_{12}^{ϕ} [kW]	I_{12}^{ϕ} [A]	ΔP_{12}^{ϕ}	ΔI_{12}^{ϕ}
Phase-A	1341.6	230.1	0.00	0.00
Phase-B	2096.0	345.7	0.00	0.00
Phase-C	2672.4	455.1	0.00	0.00

Table IX
SUMMARY OF TEST CASES (IEEE 4-NODE TEST SYSTEM)

Connection	Branch Meas.	Load Error [%]	Max. Voltage Error [%]
Yg-Yg	(P,Q)	–10	0.05
		+10	0.04
		–20	0.05
		+20	0.05
	(P,I)	–10	0.05
		+10	0.04
		–20	0.05
		+20	0.05
△-Yg	(P,Q)	–10	1.03
		+10	0.97
		–20	2.16
		+20	1.89
	(P,I)	–10	0.81
		+10	0.70
		–20	1.84
		+20	1.30
oYg-o△	(P,Q)	–10	0.01
		+10	0.03
		–20	0.04
		+20	0.05
	(P,I)	–10	0.13
		+10	0.28
		–20	0.11
		+20	0.79

B. IEEE 123-node Test System

This section reports results using the IEEE 123-node test feeder [22], with the SCADA measurement set available in Table X. The load measurements, which are not shown in the table, are pseudo-measurements representing forecast values. The SCADA measurements that can be used by the load estimator [7] and the proposed DSSE method are the per-phase real (p-a/p-b/p-c) and reactive (q-a/q-b/q-c) branch power measurements and current magnitude (I-a/I-b/I-c) measurements; they are shown as the first 18 measurements above the line in Table X. With these SCADA measurements, the load estimator [7] requires partitioning the network into four areas, as shown in Fig. 8. The measurements below the line in Table X (No. 19-28) are other practically available measurements that cannot be processed by the load estimator [7], but which can be accounted for via the industrial grade models in the proposed DSSE method; these measurements include cumulative real and reactive branch power measurements (P-abc/Q-abc), and line-to-ground (V-a/V-b/V-c) and line-to-line (V-ab/V-bc/V-ca) voltage magnitude measurements. The results from both the

This article has been accepted for publication in a future issue of this journal, but has not been fully edited. Content may change prior to final publication. Citation information: DOI 10.1109/TSG.2016.2592978, IEEE Transactions on Smart Grid

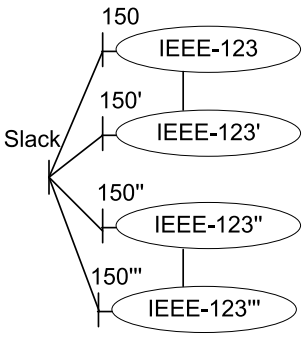

Fig. 9. Network comprised of four IEEE 123-node systems in addition to a slack node.

Table X
COMPARISON OF ESTIMATION RESULTS (IEEE 123-NODE TEST SYSTEM)

From	To	Type	SCADA	Unit	Ref. [7]		Proposed DSSE	
					EST.	Error [%]	EST.	Error [%]
150	149	p-a	1437.7	kW	1428.6	0.63	1446.8	0.63
150	149	p-b	942.6	kW	913.9	3.04	954.2	1.23
150	149	p-c	1185.3	kW	1153.6	2.67	1198.6	1.12
150	149	q-a	780.7	kVAr	772.8	1.01	782.6	0.24
150	149	q-b	435.4	kVAr	407.7	6.36	439.2	0.87
150	149	q-c	527.9	kVAr	495.6	6.12	533.3	1.02
150	149	I-a	681.2	A	676.3	0.72	679.4	0.26
150	149	I-b	432.3	A	416.6	3.63	427.2	1.18
150	149	I-c	540.2	A	522.8	3.22	532.3	1.46
13	152	I-a	360.8	A	375.6	4.10	360.3	0.14
13	152	I-b	267.1	A	258.4	3.26	266.7	0.15
13	152	I-c	292.4	A	286.3	2.09	292.3	0.03
54	57	I-a	306.5	A	321.4	4.86	306.7	0.07
54	57	I-b	257.5	A	248.9	3.34	257.4	0.04
54	57	I-c	292.4	A	286.3	2.09	292.2	0.07
72	76	I-a	129.5	A	132.6	2.39	129.5	0.00
72	76	I-b	136.2	A	137.1	0.66	136.2	0.00
72	76	I-c	99.1	A	100.2	1.11	99.3	0.20
13	18	P-abc	1084.2	kW	1025.7	5.40	1082.8	0.13
13	18	Q-abc	632.4	kVAr	638.5	0.96	631.5	0.14
1		V-a	2.292	kV	2.263	1.27	2.282	0.44
1		V-b	2.394	kV	2.338	2.34	2.392	0.08
1		V-c	2.364	kV	2.309	2.33	2.368	0.17
67		V-ab	3.915	kV	3.768	3.75	3.916	0.03
67		V-bc	4.123	kV	3.927	4.75	4.123	0.00
67		V-ca	4.077	kV	3.818	6.35	4.076	0.02
14		V-a	2.062	kV	2.213	7.32	2.074	0.58
26		V-ca	4.067	kV	3.868	4.89	4.061	0.15

Table XI
DSSE COMPUTATIONAL PERFORMANCE

Network	Iter.	Time [ms]
IEEE-4	2	1.4
IEEE-13	6	13.2
IEEE-123	4	36.1
2×IEEE-123+1	4	82.7
4×IEEE-123+1	4	104.6

load estimator [7] and the proposed DSSE method are given in the last four columns of Table X, and show that the estimated values (EST.) from the proposed estimator have significantly lower percentage error (Error) because of the SCADA measurements (below the line in Table X) that are accounted for in the model.

C. Computational Performance

The computational performance of the DSSE software was tested using 64-bit C++ implementation binaries running on Windows 8.1 with Intel i5-4690 (4x3.5-3.9GHz) and 16 GB RAM. The execution time was measured for the IEEE 4-, 13-, and 123-node networks, in addition to two networks formed by replicating the IEEE 123-node network 2 times (upper 2 networks in Fig. 9) and 4 times (4 networks in Fig. 9). The resulting computing time is shown in Table XI, and shows that the computational performance of the proposed DSSE scales well with problem size.

V. CONCLUSION

This paper presented the implementation details of an equality-constrained WLS method that can calculate the state of real-life operational distribution networks. The proposed DSSE method handles delta loads, all possible transformer connection types, voltage drop regulators with ganged and per-phase Y/△ load tap-changing transformers, cumulative power measurements, line-to-ground and line-to-line voltage magnitude measurements, and multiphase branches in radial/meshed topology. These characteristics positively distinguish the proposed estimation method from classical and recent implementations, in addition to a state-of-the-art method for load estimation in radial and unsymmetrical distribution networks. The program files of the implementation are made available for follow-up research.

REFERENCES

[1] I. Roytelman and S. M. Shahidehpour, "Practical aspects of distribution automation in normal and emergency conditions," *IEEE Trans. Power Deliv.*, vol. 8, no. 4, pp. 2002–2008, Oct. 1993.

[2] A. K. Ghosh, D. L. Lubkeman, and R. H. Jones, "Load modeling for distribution circuit state estimation," *IEEE Trans. Power Deliv.*, vol. 12, no. 2, pp. 999–1005, Apr. 1997.

[3] D. L. Lubkeman, J. Zhang, A. K. Ghosh, and R. H. Jones, "Field results for a distribution circuit state estimator implementation," *IEEE Trans. Power Deliv.*, vol. 15, no. 1, pp. 399–406, Jan. 2000.

[4] E. Manitsas, R. Singh, B. C. Pal, and G. Strbac, "Distribution system state estimation using an artificial neural network approach for pseudo measurement modeling," *IEEE Trans. Power Syst.*, vol. 27, no. 4, pp. 1888–1896, Nov. 2012.

[5] B. P. Hayes, J. K. Gruber, and M. Prodanovic, "A closed-loop state estimation tool for MV network monitoring and operation," *IEEE Trans. Smart Grid*, vol. 6, no. 4, pp. 2116–2125, Jul. 2015.

[6] M. R. Irving and C. N. Macqueen, "Robust algorithm for load estimation in distribution networks," *IEE Proc.-Gener. Transm. and Distrib.*, vol. 145, no. 5, pp. 499–504, Sep. 1998.

[7] I. Džafić, M. Gilles, R. A. Jabr, B. C. Pal, and S. Henselmeyer, "Real time estimation of loads in radial and unsymmetrical three-phase distribution networks," *IEEE Trans. Power Syst.*, vol. 28, no. 4, pp. 4839–4848, Nov. 2013.

[8] I. Roytelman and S. M. Shahidehpour, "State estimation for electric power distribution systems in quasi real-time conditions," *IEEE Trans. Power Deliv.*, vol. 8, no. 4, pp. 2009–2015, Oct. 1993.

[9] M. E. Baran and A. W. Kelley, "State estimation for real-time monitoring of distribution systems," *IEEE Trans. Power Syst.*, vol. 9, no. 3, pp. 1601–1609, Aug. 1994.

[10] ——, "A branch-current-based state estimation method for distribution systems," *IEEE Trans. Power Syst.*, vol. 10, no. 1, pp. 483–491, Feb. 1995.

[11] S. Nanchian, A. Majumdar, and B. C. Pal, "Three-phase state estimation using hybrid particle swarm optimization," *IEEE Trans. Smart Grid - Early Access*, 2015.

[12] J. B. Leite and J. R. S. Mantovani, "Distribution system state estimation using the hamiltonian cycle theory," *IEEE Trans. Smart Grid*, vol. 7, no. 1, pp. 366–375, Jan. 2016.
[13] M. K. Celik and W.-H. E. Liu, "A practical distribution state calculation algorithm," in *IEEE Power Engineering Society Winter Meeting*, vol. 1, Jan. 1999, pp. 442–447.
[14] J. Wu, Y. He, and N. Jenkins, "A robust state estimator for medium voltage distribution networks," *IEEE Trans. Power Syst.*, vol. 28, no. 2, pp. 1008–1016, May 2013.
[15] I. Džafić, R. A. Jabr, and H.-T. Neisius, "Transformer modeling for three-phase distribution network analysis," *IEEE Trans. Power Syst.*, vol. 30, no. 5, pp. 2604–2611, Sep. 2015.
[16] *BS EN 60076-1: 2011: Power transformers - general*. British Standards Institute, 2011.
[17] J. Arrillaga and C. P. Arnold, *Computer analysis of power systems*. Chichester, England: Wiley, 1990.
[18] W. H. Kersting, *Distribution system modeling and analysis*. Boca Raton, FL: CRC Press, 2002.
[19] A. Abur and A. Gómez Expósito, *Power System State Estimation: Theory and Implementation*. New York, NY: Marcel Dekker, 2004.
[20] R. Baldick, *Applied Optimization: Formulation and Algorithms for Engineering Systems*. Cambridge, UK: Cambridge University Press, 2006.
[21] I. Džafić, I. Huseinagić, and R. A. Jabr, "DNToolbox version 1.0.0," https://sites.google.com/site/dntoolbox/, accessed: 2016-6-24.
[22] IEEE PES Distribution System Analysis Subcommittee, "Distribution test feeders," http://ewh.ieee.org/soc/pes/dsacom/testfeeders/, accessed: 2016-06-24.
[23] "DSSE results for the IEEE 4-node test feeder," https://dl.dropboxusercontent.com/u/47198710/DSSE_Results_IEEE4.xlsx, accessed: 2016-6-24.

Izudin Džafić (M'05-SM'13) received his Ph.D. degree from University of Zagreb, Croatia in 2002. He is currently an Associate Professor in the Department of Electrical Engineering at the International University of Sarajevo, Bosnia. From 2002 to 2014, he was with Siemens AG, Nuremberg, Germany, where he held the position of the Head of the Department and Chief Product Owner (CPO) for Distribution Network Analysis (DNA) R&D. His research interests include power system modeling, development and application of fast computing to power systems simulations. Dr. Džafić is a member of the IEEE Power and Energy Society and the IEEE Computer Society.

Rabih Jabr (M'02-SM'09-F'16) was born in Lebanon. He received the B.E. degree in electrical engineering (with high distinction) from the American University of Beirut, Beirut, Lebanon, in 1997 and the Ph.D. degree in electrical engineering from Imperial College London, London, U.K., in 2000. Currently, he is a Professor in the Department of Electrical and Computer Engineering at the American University of Beirut. His research interests are in mathematical optimization techniques and power system analysis and computing.

Indira Huseinagić received the electrical engineering B.Sc. and M.Sc. degrees from the University of Sarajevo, Bosnia and Herzegovina, in 2008 and 2010, respectively. She is currently a Senior Assistant and Ph.D. student in the Electrical and Electronics Engineering department, International University of Sarajevo. Her research interests include analysis and optimization of power systems.

Bikash C. Pal (M'00-SM'02-F'13) received the B.E.E. (with honors) degree from Jadavpur University, Calcutta, India, the M.E. degree from the Indian Institute of Science, Bangalore, India, and the Ph.D. degree from Imperial College London, London, U.K., in 1990, 1992, and 1999, respectively, all in electrical engineering. Currently, he is a Professor in the Department of Electrical and Electronic Engineering, Imperial College London. His current research interests include state estimation, power system dynamics, and flexible ac transmission system controllers.